ARTICLE

Imaging the Dissociation Dynamics of Si_2^+ via Two-Photon Excitation at 193 nm†

Yu-jie Ma, Fang-fang Li, Jia-xing Liu, Feng-yan Wang*

Department of Chemistry and Shanghai Key Laboratory of Molecular Catalysis and Innovative Materials, Collaborative Innovation Center of Chemistry for Energy Materials (iChEM), Fudan University, Shanghai 200433, China

(Dated: Received on January 13, 2019; Accepted on January 22, 2019)

In the one-color experiment at 193 nm, we studied the photodissociation of Si_2^+ ions prepared by two-photon ionization using the time-sliced ion velocity map imaging method. The Si^+ imaging study shows that Si_2^+ dissociation results in two distinct channels: $Si(^3P_g)+Si^+(^2P_u)$ and $Si(^1D_2)+Si^+(^2P_u)$. The main channel $Si(^3P_g)+Si^+(^2P_u)$ is produced by the dissociation of the Si_2^+ ions in more than one energetically available excited electronic state, which are from the ionization of $Si_2(v=0-5)$. Particularly, the dissociation from the vibrationally excited $Si_2(v=1)$ shows the strongest signal. In contrast, the minor $Si(^1D_2)+Si^+(^2P_u)$ channel is due to an avoided crossing between the two $^2\Pi_g$ states in the same symmetry. It has also been observed the one-photon dissociation of $Si_2^+(X^4\Sigma_g^-)$ into $Si(^1D_2)+Si^+(^2P_u)$ products with a large kinetic energy release.

Key words: Slice imaging, Photodissociation, Silicon dimmer Si_2, 193 nm

I. INTRODUCTION

Silicon is abundant in interstellar space and silicon materials are important to semiconductor industry. Over the past four decades, the properties of small silicon clusters have received a great deal of interest in order to understand how their structure and properties evolve with size [1]. As a first step in understanding the nature of electronic states in large clusters, there have been numerous experimental and theoretical studies reported on the spectroscopic and electronic states of the simple yet important Si_2 dimers [2−18]. In these studies, most focused on the potential energy surfaces on the neutral Si_2 molecules, and there were only a few studies on the electronic structure of Si_2^+.

Combined with theoretical and experimental studies, the ground state of neutral Si_2 is $X^3\Sigma_g^-(\sigma_u^2\pi_u^2\sigma_g^2)$, and the lowest excited $1^3\Pi_u(\sigma_u^2\pi_u^3\sigma_g)$ state is located at T_e=669 cm^{-1} [7, 19]. Considering both $X^3\Sigma_g^-$ and $1^3\Pi_u$ of Si_2, which have nearly equal minimal energies, the ground states of the neutral and ionic species are related by a direct σ_g or π_u ionization in Si_2. Specifically, the ground state of the Si_2^+ is $X^4\Sigma_g^-(\sigma_u^2\pi_u^2\sigma_g)$ and the first excited $1^2\Pi_u(\sigma_u^2\pi_u\sigma_g^2)$ state lies at T_e=4194 cm^{-1} (0.52 eV) [10, 15]. Dixon and coworkers studied the role of excited states of Si_2 in photoionization [15]. Marijnissen and ter Meulen used the N $^3\Sigma_u^-$ state at 46763 cm^{-1} (5.80 eV) as the intermediate state in the two-photon ionization process of Si_2 and measured its ionization potential at 63884 cm^{-1} (7.92 eV) [20]. Sefyani and Schamps calculated the lowest-lying Rydberg state of Si_2 in the range of 35000−55000 cm^{-1} (4.34−6.82 eV) [15]. For the electronic states of Si_2^+ ions, Bruna and co-workers predicted series of potential curves of the electron configurations which dissociate into $Si(^3P_g)+Si^+(^2P_u)$ through large-scale *ab initio* CI calculations [10]. Liu *et al.* performed *ab initio* all-electron relativistic calculations of the low-lying excited states of Si_2^+ with and without consideration of spin-orbit interaction on Si_2^+ [21].

The previous experimental and theoretical studies have provided details on the spectroscopy and thermodynamics properties of Si_2 dimers. However, to the best of our knowledge, we found no experiments on the photodissociation dynamics of silicon dimers. In this work, the photodissociation of Si_2^+ molecule prepared by two-photon ionization at 193 nm was studied by using time-sliced ion velocity map imaging method. Two types of ionic photodissociation channels $Si(^3P_g)+Si^+(^2P_u)$ and $Si(^1D_2)+Si^+(^2P_u)$ were observed and more details on the related dissociation mechanisms are given below.

II. EXPERIMENTS

The photodissociation experiment of Si_2^+ at 193 nm was performed in self-designed crossed-molecular beam

†Dedicated to Professor Kopin Liu on the occasion of his 70th birthday.

*Author to whom correspondence should be addressed. E-mail: fengyanwang@fudan.edu.cn

setup and only one molecular beam was used in the present experiment [22−24]. Briefly, the Si_2 molecules were generated by laser ablation on a silicon rod at 532 nm, which was produced by frequency-doubling of the output of Continuum Minilite II. Then the ablated Si_2 molecules were seeded in a supersonic argon gas beam formed via an Even-Lavie valve and expanded into the main vacuum chamber. The free expansion design in the laser ablation source allows the generation of mainly ablated atoms and small clusters [22]. In the center of ion optics region, the Si_2 molecular beam intersected with a linearly polarized laser pulse at 193 nm (∼0.3 mJ) generated by an excimer laser (GAM-Laser, Inc. EX5), which was focused by a circular convex lens (f=50 cm). A Brewster window was used to set the polarization of the laser. Under the action of the ion optics system with a total voltage of 1800 V, the produced ions were accelerated to the position sensitive detector, which is composed of two microchannel plates (MCP, 75 mm diameter, Photek) and one Phosphor Screen (P43, Photek). Finally, the center slice of Si^+ ion cloud was gated by adding a 30 ns pulse width on the back MCP and the emitted light from P43 was captured by the Lavision Elite CCD camera. The image was acquired and processed by an improved software "Davis 8.2".

III. RESULTS AND DISCUSSION

The raw slice image of Si^+ ions from one color experiment at 193 nm is shown in FIG. 1. The Si^+ ions lying near the center and having a speed of almost zero are ionized Si monomers generated by laser ablation of Si rod, and the Si^+ ions having a recoil speed are produced from the dissociation process. As the Si^+ speed increases in FIG. 1, four distinct dissociation channels appear, marking regions A, B, C and D, respectively. The linear polarization direction of the laser is shown in FIG. 1. We define θ as the angle between the polarization vector of the photolysis laser and the recoil velocity vector of the product. By integrating the signal over the θ=0°−360° angular range, the corresponding speed distribution is present in FIG. 2(a). In order to obtain better speed resolution, the integrated speed distribution in the small angular range of θ=0°−5° is shown in FIG. 2(b), and clear vibrational structures are resolved in regions B and C. The species observed in the molecular beam are mainly Si^+ and $Si_2{}^+$, and trace amounts of SiO^+. The Si^+ ions in the region A are related to the dissociation of SiO, and when the carrier gas of argon is changed to O_2, the dissociation channel of SiO in region A becomes stronger. The dissociation dynamics of silicon oxide will be discussed in detail in the next paper and will therefore not be discussed in this work. The sharp rings of Si^+ with large recoil velocity in regions B, C and D are related with the dissociation dynamics of silicon dimmer, which is the focus of this paper. The

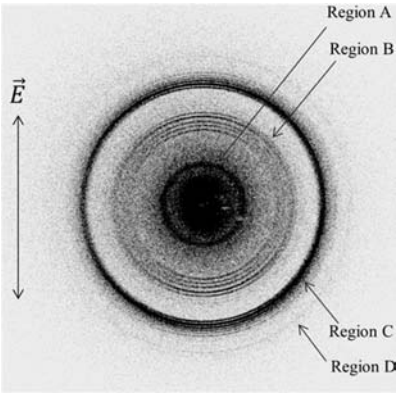

FIG. 1 Raw slice image of Si^+ ions from the one-color experiment at 193 nm. As the radius of the ring increases, four distinct dissociation pathways are divided into four regions.

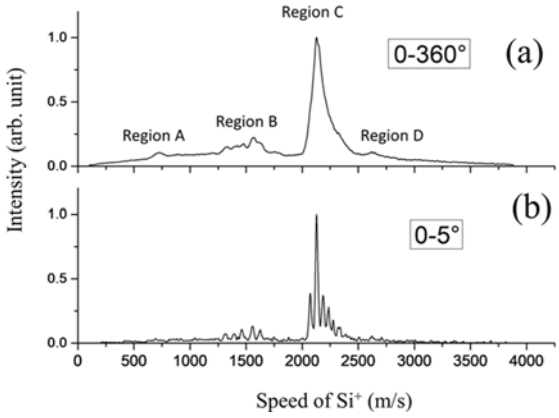

FIG. 2 Speed distributions of Si^+ ions obtained by integrating the signals over (a) the whole angular range (0°−360°) and (b) a small angular range (0°−5°), where the integration of a small angle gives a better speed resolution.

similar ring structure in regions B and C reflects the vibrational excitation of the parent molecule, *i.e.*, silicon dimmer.

According to the recoil momentum conservation in $Si_2/Si_2{}^+$ photodissociation, the speed distribution of Si^+ is converted to the total kinetic energy release (TKER) distribution of Si^++Si, as shown in FIG. 3. The TKER interval between adjacent peaks in regions B and C respectively is approximately 500 cm^{-1}, which is consistent with the experimental obtained vibrational frequency (511 cm^{-1}) of the $Si_2(X^3\Sigma_g^-)$ molecule [25]. The first excited electronic state of $Si_2(D\ ^3\Pi_u)$ of the low energy level (T_e=669 cm^{-1}) can also be involved in photon excitation, where the vibrational frequency ω_e=536 cm^{-1} and the equilibrium inter-nuclear distance R_e=2.12 Å (comparatively, 2.25 Å for $X^3\Sigma_g^-$) [7]. The first peak in region C has a total kinetic energy release of 10030 cm^{-1} which is about 6000 cm^{-1} higher than the first peak at 4030 cm^{-1} in region B. The energy analysis shows that the signals in regions B

DOI:10.1063/1674-0068/cjcp1901011

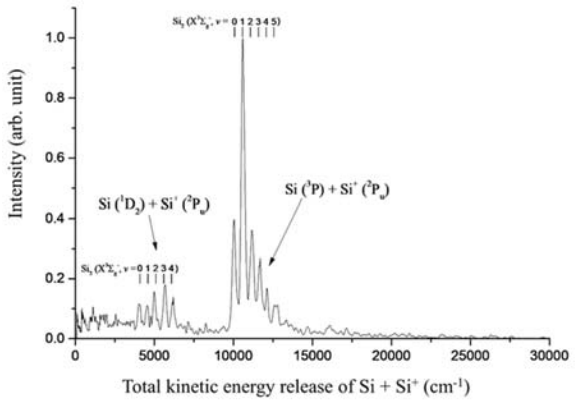

FIG. 3 The total kinetic energy release distribution of Si+Si^+ products converted from FIG. 2(b). The assignments of vibrational structures of Si_2 are shown in the two channels, $Si(^3P_g)+Si^+(^2P_u)$ and $Si(^1D_2)+Si^+(^2P_u)$, respectively.

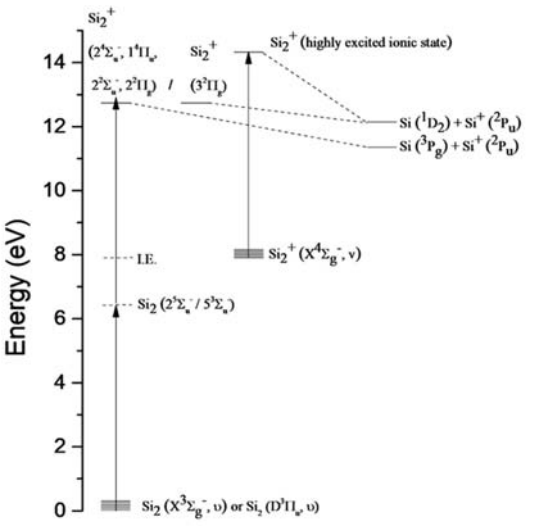

FIG. 4 The associated channels for the formation of Si^+ products from Si_2^+ ions.

(C) come from the dissociation of Si_2^+ ions after two-photon ionization of Si_2 of v=0−4 (v=0−5), as shown in FIG. 3. The ionization potential energy of $Si_2(X^3\Sigma_g^-)$ is 7.92 eV, requiring two photons at 193 nm to ionize the ground $Si_2(X^3\Sigma_g^-)$ state. The processes involved in the two-photon absorption are

$$Si_2(X^3\Sigma_g^-, v) \xrightarrow{2h\nu} Si(^1D_2)+Si^+(^2P_u)+e\,(\text{region B}) \quad (1)$$

$$\xrightarrow{2h\nu} Si(^3P_g)+Si^+(^2P_u)+e\,(\text{region C}) \quad (2)$$

Based on energy conservation, the available energy for the ionic dissociation channel is shown as

$$\begin{aligned} &2h\nu + E_{\text{int}}(Si_2) - \text{IE}(Si_2) - D_0(Si_2^+) \\ &= E_{\text{int}}(Si^+ + Si) + E_{\text{KER}}(e^- + Si^+ + Si) \end{aligned} \quad (3)$$

where the two-photon excitation energy $2h\nu$= 103627 cm^{-1} (12.85 eV), $E_{\text{int}}(Si_2)$ is the internal energy of Si_2, $\text{IE}(Si_2)$ is the ionization energy of Si_2, *i.e.*, 63884 cm^{-1} (7.92 eV) [20], $D_0(Si_2^+)$ is the ground state dissociation energy of Si_2^+, *i.e.*, 28827 cm^{-1} (3.57 eV) [21], $E_{\text{int}}(Si^+ + Si)$ is the electronic energy of Si^+ and Si products, 6298.85 cm^{-1} for $Si^+(^2P_u)+Si(^1D_g)$ channel and 0 for $Si^+(^2P_u)+Si(^3P_g)$ channel, and $E_{\text{KER}}(e^- + Si^+ + Si)$ is the translational energy distributed in the Si^+, Si and electrons. The internal energy difference between the $Si^+(^2P_u)+Si(^1D_2)$ and $Si^+(^2P_u)+Si(^3P_g)$ channels is 6298.85 cm^{-1} which is consistent with the observation of the TKER difference between the two channels for $Si_2(X^3\Sigma_g^-$, v=0).

As shown in FIG. 3, the channel of $Si^+(^2P_u)+Si(^3P_g)$ from the excitation of $Si_2(X^3\Sigma_g^-$, v=0) has the TKER of 10030 cm^{-1}, and corresponds to the electron recoil energy about 886 cm^{-1} according to Eq.(3). Hence the energy analysis indicates that, according to the Franck-Condon factors, one or even more than one repulsive state of Si_2^+ with T_v≈38857 cm^{-1} (4.82 eV) is involved in the dissociation at R≈2.246 Å (the equilibrium bond length of the ground Si_2). Meanwhile, the repulsive excited state of Si_2^+ has an avoided crossing with another electronic state in the same symmetry, and then the $Si^+(^2P_u)+Si(^1D_2)$ channel is also observed.

The peak in region D has a total kinetic energy release of 16000 cm^{-1}. The energy analysis shows that the Si^+ ions in region D are from the one-photon dissociation of $Si_2^+(X^4\Sigma_g^-)$, which is produced by two-photon ionization of $Si_2(X^3\Sigma_g^-)$. The process is:

$$Si_2(X^3\Sigma_g^-) \xrightarrow{2h\nu} Si_2^+(X^4\Sigma_g^-) + e^- \quad (4)$$

$$Si_2^+(X^4\Sigma_g^-) \xrightarrow{h\nu} Si(^1D_2) + Si^+(^2P_u) \quad (5)$$

Based on energy conservation, the TKER of $Si(^1D_2)+Si^+(^2P_u)$ fragments will be simplified as

$$E_{\text{TKER}}(Si^+ + Si) = h\nu - D_0(Si_2^+) - E_{\text{int}}(Si^+ + Si) \quad (6)$$

where $E_{\text{TKER}}(Si^+ + Si)$ is the total kinetic energy release in the $Si(^1D_2)+Si^+(^2P_u)$ products, $h\nu$ is 51813.5 cm^{-1}, $D_0(Si_2^+)$ is the ground state dissociation energy of Si_2^+, *i.e.*, 28827 cm^{-1} (3.57 eV), and $E_{\text{int}}(Si^+ + Si)$ is the internal energy of $Si(^1D_2)+Si^+(^2P_u)$ products, *i.e.*, 6298.85 cm^{-1} (0.78 eV). Then the total kinetic energy E_{TKER} for the $Si(^1D_2)+Si^+(^2P_u)$ products is predicted to be approximately 16688 cm^{-1}, which is consistent with the measured TKER of 16440 cm^{-1}. The slight energy difference of 250 cm^{-1} can be attributed to the excitation of the spin-orbit coupling state of $Si^+(^2P_{3/2})$ (287.24 cm^{-1} above the $^2P_{1/2}$ state). Considering that the channel in region D requires more photons in the associated dissociation dynamics than the channels in regions B and C, it is reasonable to observe a relatively weak signal in this region.

According to the two theoretical calculations by Bruna *et al.* [10] and Liu *et al.* [21], more than one

DOI:10.1063/1674-0068/cjcp1901011

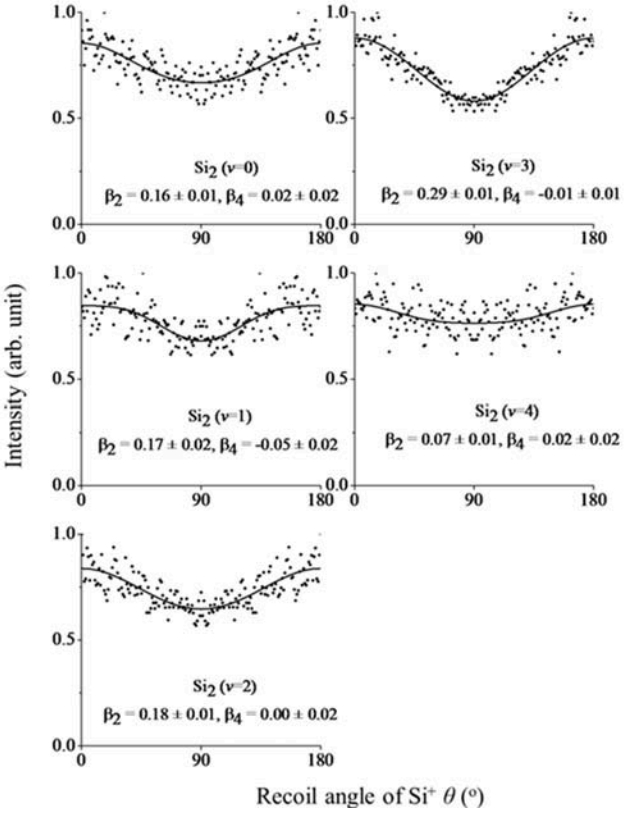

FIG. 5 The angular distributions of the peaks observed in region B of FIG. 2(b). The solid lines represent fits to the measured angular distributions using Eq.(7).

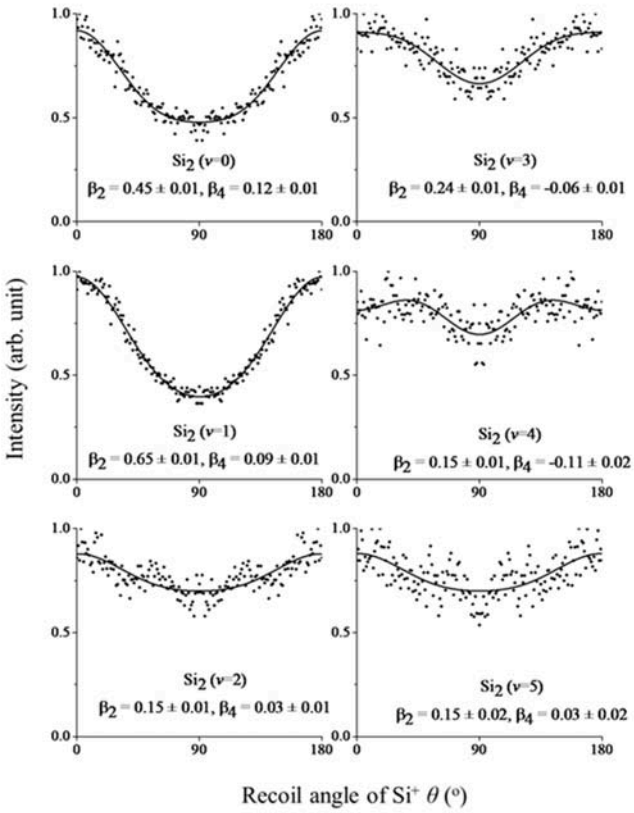

FIG. 6 The angular distributions of the peaks observed in region C of FIG. 2(b). The solid lines represent fits to the measured angular distributions using Eq.(7).

of the excited potential curves of ionic state can be involved in the ionic dissociation into $Si(^3P_g)+Si^+(^2P_u)$. According to the information of the excited electronic state obtained above, that is, $T_v\approx38857$ cm^{-1}(4.82 eV) at the bond length of $R\approx2.25$ Å, compared with the potential energy curves of Liu *et al.* [21], the repulsive doublet $2^2\Sigma_u^-$ state and the quartet $2^4\Sigma_u^-$ and $1^4\Pi_u$ states can be involved in the ionic dissociation. In the work of Bruna *et al.* [10], in addition to the contributions of quartet $2^4\Sigma_u^-$ ($T_v\approx4.59$ eV at $R\approx2.33$ Å), $1^4\Pi_u$($T_v\approx4.94$ eV at $R\approx2.33$ Å) and doublet $2^2\Sigma_u^-$($T_v\approx4.56$ eV at $R\approx2.33$ Å) states, the doublet $2^2\Pi_g$ state($T_v\approx3.94$ eV at $R\approx2.33$ Å) can also contribute to the dissociation of $Si(^3P_g)+Si^+(^2P_u)$. Bruna *et al.* predicted that the energy of $2^2\Pi_g$ state decreases suddenly at large distance due to the avoided crossing with the $3^2\Pi_g$ state, which is decomposed into $Si(^1D_2)+Si^+(^2P_u)$. The role of $2^2\Pi_g$ state helps to explain the $Si(^1D_2)+Si^+(^2P_u)$ channel. For clarity, FIG. 4 shows the associated channels for the formation of Si^+ ions from $Si_2{}^+$. In the present experimental data, we cannot distinguish the exact Ω state of the $Si^+(^2P_\Omega)$ state, and therefore the spin-orbit coupling is generally not considered in the present discussion.

For the (1+1) ionization of Si_2, the possible intermediate state $2^5\Sigma_u^-$ or $5^3\Sigma_u^-$ near the one-photon energy of 193 nm has the equilibrium bond length $R_e\approx2.35(6)$ Å [15]. Since the equilibrium bond length of the excited state is significantly longer than that of the ground state, the Franck-Condon transition occurs when the ground state and the intermediate state are in excited vibrational states. Moreover, the Franck-Condon factors occurs in the transition from the intermediate states to the final electronic states. Therefore, according to the Franck-Condon principle, it can be understood that the strongest $Si(^3P_g)+Si^+(^2P_u)$ products are produced from the vibrationally excited $Si_2{}^+(v=1)$ and the most intense $Si(^1D_2)+Si^+(^2P_u)$ are from the vibrationally excited $Si_2{}^+(v=3)$ state.

The angular distributions of Si^+ ions in regions B and C are shown in FIG. 5 and FIG. 6, respectively. The angular distribution of photofragment produced from the two-photon photolysis of unaligned molecules with a linearly polarized laser can be expressed as [26]

$$I(\theta) = I_0\left[1+\sum_1^n \beta_{2n}P_{2n}(\cos\theta)\right] \qquad (7)$$

where n is the number of photons involved in photolysis, and n=2 in regions B and C, and β_{2n} is a coefficient that weights contributions from various order P_{2n} Legendre polynomials. The parameters β_2 and β_4 are fitted by

DOI:10.1063/1674-0068/cjcp1901011

Eq.(7) and are shown in FIG. 5 and FIG. 6. It can be easily seen from the figures that the experimental data are well fitted. The small anisotropy parameters obtained for the regions B and C can be explained if we consider that more than one potential energy surface is involved in the parent ion dissociation that leads to the production of this channel, but also if the dissociation to the channel is slow compared to the rotational period of the parent ion.

IV. CONCLUSION

Two types of the ionic dissociation after the two-photon ionization of Si_2 molecules at 193 nm were observed by using time-sliced velocity map imaging technique. One leads to $Si(^3P_g)+Si^+(^2P_u)$, and the other is $Si(^1D_2)+Si^+(^2P_u)$. More than one excited electronic state of Si_2^+ obtained by two-photon ionization can directly produce $Si(^3P_g)+Si^+(^2P_u)$ channel. The avoided crossing between two excited electronic states in the same symmetry was contributed to the $Si(^1D_2)+Si^+(^2P_u)$ channel. In order to better understand the dissociation dynamics of Si_2/Si_2^+ molecules, more studies on Si_2/Si_2^+ photodissociation in the ultraviolet region will be reported.

V. ACKNOWLEDGMENTS

This work was supported by the National Natural Science Foundation of China (No.21673047, No.21327901, and No.21322309), the Shanghai Key Laboratory Foundation of Molecular Catalysis and Innovative Materials, and the Program for Professor of Special Appointment (Eastern Scholar) at Shanghai Institutions of Higher Learning.

[1] K. Raghavachari, Phase Transitions **24-26**, 61 (1990).
[2] A. E. Douglas, Can. J. Phys. **33**, 801 (1955).
[3] R. D. Verma and P. A. Warsop, Can. J. Phys. **41**, 152 (1963).
[4] D. E. Milligan and M. E. Jacox, J. Chem. Phys. **52**, 2594 (1970).
[5] A. Lagerqvist and C. Malmberg, Phys. Scr. **2**, 45 (1970).
[6] I. Dubois and H. Leclercq, Can. J. Phys. **49**, 3053 (1971).
[7] T. N. Kitsopoulos, C. J. Chick, Y. Zhao, and D. M. Neumark, J. Chem. Phys. **95**, 1441 (1991).
[8] K. S. Ojha and R. Gopal, Spectrochim. Acta-Part A **71**, 1003 (2008).
[9] C. C. Arnold, T. N. Kitsopoulos, and D. M. Neumark, J. Chem. Phys. **99**, 766 (1993).
[10] P. J. Bruna, C. Petrongolo, R. J. Buenker, and S. D. Peyerimhoff, J. Chem. Phys. **74**, 4611 (1981).
[11] S. D. Peyerimhoff and R. J. Buenker, Chem. Phys. **72**, 111 (1982).
[12] J. E. Northrup, M. T. Yin, and M. L. Cohen, Phys. Rev. A **28**, 1945 (1983).
[13] P. J. Knowles and H. J. Werner, Chem. Phys. Lett. **115**, 259 (1985).
[14] K. Raghavachari, J. Chem. Phys. **84**, 5672 (1985).
[15] F. L. Sefyani and J. Schamps, Chem. Phys. **191**, 155 (1995).
[16] D. A. Dixon, D. Feller, K. A. Peterson, and J. L. Gole, J. Phys. Chem. A **104**, 2326 (2000).
[17] E. L. Snow and S. R. Lundeen, Phys. Rev. A **75**, 062512 (2007).
[18] D. H. Shi, H. Liu, J. F. Sun, Z. L. Zhu, and Y. F. Liu, J. Quant. Spectrosc. Radiat. Transfer **112**, 2567 (2011).
[19] P. J. Bruna, S. D. Peyerimhoff, and R. J. Buenker, J. Chem. Phys. **72**, 5437 (1980).
[20] A. Marijnissen and J. J. ter Meulen, Chem. Phys. Lett. **263**, 803 (1996).
[21] Y. L. Liu, H. S. Zhai, X. M. Zhang, and Y. F. Liu, Chem. Phys. **425**, 156 (2013).
[22] C. W. Dong, J. X. Liu, F. F. Li, and F. Y. Wang, Chin. J. Chem. Phys. **29**, 99 (2016).
[23] F. Li, C. Dong, J. Chen, J. Liu, F. Wang, and X. Xu, Chem. Sci. **9**, 488 (2018).
[24] F. Li, Y. Ma, J. Liu, and F. Wang, J. Chem. Phys. **149**, 124303 (2018).
[25] H. G. M. S. a. M. S. I. Huber KP, *Constants of Diatomic Molecules. Princeton*, NJ: Van Nostrand Reinhold, (1979) and references therein.
[26] R. N. Dixon, J. Chem. Phys. **122**, 194302 (2005).

DOI:10.1063/1674-0068/cjcp1901011